journal

Theory and Modeling of Glasses and Ceramics

J. Am. Ceram. Soc., **81** [3] 492–500 (1998)

Three-Dimensional Computer Simulation of Ferroelectric Domain Formation

Hong-Liang Hu* and Long-Qing Chen

Department of Materials Science and Engineering, The Pennsylvania State University, University Park, Pennsylvania 16802

Three-dimensional (3-D) computer simulations of ferroelectric domain formation and evolution were performed, using a computer simulation model based on the time-dependent Ginsburg–Landau equations. A cubic-to-tetragonal ferroelectric phase transition is considered. It is shown that the initial stage of the transition during the annealing of a quenched cubic paraelectric phase involves the nucleation and growth of the ferroelectric domains, followed by the domain coarsening leading to the formation of 90° and 180° domain structures. Part of the 3-D results reported here confirm our conclusions made earlier for the two-dimensional (2-D) case, namely, the nonlocal elastic interactions are critical to the formation of twin structure and the dipole–dipole interactions are responsible for the head-to-tail arrangements of dipoles at twin boundaries. In contrast to our previous work, and others; the effect of the depolarization energy was explicitly incorporated into the simulation model. It is found that when there are no surface charges to compensate the Lorentz field due to the polarization charges, and if the system is mechanically clamped, both 90° and 180° domains are thermodynamically stable.

I. Introduction

A COMMON feature of ferroelectric ceramics[1–4] is the formation of domain structures when a paraelectric phase is cooled through the ferroelectric transition temperature. The crystallographic and thermodynamic aspects of domain structures are reasonably understood. However, essentially all the experimentally observed domain structures are nonequilibrium. They are frozen domain structures formed along the ferroelectric transformation and subsequent evolution path towards equilibrium. The formation and evolution of domain structures are much more complex and are difficult to predict analytically. On the other hand, a fundamental understanding of the domain dynamics is critical for controlling the properties such as permittivity and piezoelectricity.[4] For example, it is critical to understand the evolution of domain structures under external fields in order to control them in poled ferroelectric ceramics for use as piezoelectric transducers.

In a cubic–tetragonal transformation, there are three possible orientation variants with the tetragonal axes along [100], [010], or [001] directions, or six if we count those along opposite directions as separate variants. The number of orientation variants increases to eight if the crystalline symmetry of the ferroelectric phase is rhombohedral. In the absence of any external field, all of them have the same probability to form in the parent cubic paraelectric phase below the ferroelectric transition temperature. The corresponding microstructure of the ferroelectric phase will contain all possible domains separated by the so-called domain walls. Consequently, in the tetragonal phase it is possible that the polarization vectors in adjacent domains are perpendicular (as in the case of 90° domains) or antiparallel (180° domains) to each other across a domain wall. Depending on the relative orientation of the polarization vectors in the adjacent domains 90° domain walls can be further classified into head-to-tail and head-to-head (tail-to-tail) walls.

Experimentally, both 90° domains and 180° domains are found to coexist in many ferroelectric materials.[1–3] In the case of 90° domains, it is found that head-to-tail arrangements are predominant.

Recently there have been a number of two-dimensional (2-D) computer simulations[6–8] of domain structure evolution during ferroelectric transitions using the time-dependent Ginsburg–Landau equation (TDGL) field model. This model does not make *a priori* assumptions on the domain morphologies and their evolution path. The nonlocal elastic interactions, the electric dipole–dipole interactions, and the local interactions at domain walls are taken into account simultaneously. Preliminary studies of the dynamics of 180° and 90° domain wall formation were reported in Refs. 7 and 6, respectively. The main focus of Ref. 6 was to investigate the effect of nonlocal electric dipole–dipole interactions on the domain structures. A similar computer simulation study was done by Nambu and Sagala.[8] However, they did not take into account the long-range electric dipole–dipole interaction, which in fact was shown in Ref. 6 to be essential in predicting the formation of head-to-tail arrangement at 90° domain walls.

These previous studies have produced promising results towards a better understanding of the formation and evolution of ferroelectric domain structures. However, all of these simulations were performed in 2-D. Undoubtedly a more realistic three-dimensional (3-D) simulation is desirable. In 3-D, even the point groups are different from those in the 2-D case. Also in 3-D there is one more dimension and hence one more degree of freedom to relax the total free energy of a system. As a result, although 2-D computer simulation is valuable, we cannot make assertions confidently based on 2-D simulation alone. Furthermore, none of the previous simulations have incorporated the effect of depolarization energy on the domain structure.

In this paper, we will report our results of 3-D simulations. We will consider a cubic-to-tetragonal ferroelectric phase transition. Some of the results confirm our conclusions made earlier for the 2-D case,[6] namely, the nonlocal elastic interactions are critical to the formation of twin structure, and the dipole–dipole interactions are responsible for the head-to-tail arrangements of dipoles at twin boundaries. The effect of the depolarization energy is considered. It is found that when there are no surface charges to compensate the Lorentz field due to the polarization charges, and if a system is mechanically clamped, both 90° and 180° domains are stable.

V. Tikare—contributing editor

Manuscript No. 190934. Received June 10, 1997; approved November 25, 1997.
Presented at the 99th Annual Meeting of The American Ceramic Society, Cincinnati, OH, May 5–7, 1997 (Theory and Computational Modeling Symposium, Paper No. SXIXP-009-97).
Supported by the National Science Foundation under Grant No. DMR-96-33719. The computer simulations were performed at the Pittsburgh Superconducting Center.
*Member, American Ceramic Society.

This paper is organized as follows: In Section II, for self-content, the formulation[6] for thermodynamics of domain structures is reviewed; Section III discusses the elastic strain energy calculation; in Section IV, the so-called time–dependent Ginsburg–Landau equation is introduced; a discussion about the semiimplicit method used in this simulation is presented in Section V; the results of computer simulation are analyzed in Section VI; finally, the conclusion is contained in Section VII.

II. Thermodynamic Description of a Domain Structure

Landau theory has played an important role in understanding the thermodynamics of ferroelectric phase transitions. The free-energy density is represented by a polynomial of order parameters. For modeling the formation and the evolution of ferroelectric domains, a natural choice of order parameter is the spontaneous polarization. For an inhomogeneous system, the spontaneous polarization is spatially dependent and consequently is a vector field. In the particular example of cubic–tetragonal transition, a domain structure is described by a three-component polarization vector field $\mathbf{P} = (P_x, P_y, P_z)$. For an inhomogeneous system, the local free-energy density also becomes a function of position through the dependence on the polarization vector. Since we are interested in first-order cubic-to-tetragonal proper ferroelectric transitions, following Ref. 9, we employ a six-order polynomial for the Landau free energy.

$$\begin{aligned} f_L(P_i) = {} & \alpha_1(P_x^2 + P_y^2 + P_z^2) + \alpha_{11}(P_x^4 + P_y^4 + P_z^4) \\ & + \alpha_{12}(P_x^2P_y^2 + P_y^2P_z^2 + P_z^2P_x^2) + \alpha_{111}(P_x^6 + P_y^6 + P_z^6) \\ & + \alpha_{112}[P_x^4(P_y^2 + P_z^2) + P_y^4(P_x^2 + P_z^2) + P_z^4(P_x^2 + P_y^2)] \\ & + \alpha_{123}P_x^2P_y^2P_z^2 \end{aligned} \tag{1}$$

where $i,j = 1, 2, 3$ stand for x, y, z, respectively, and the α's will be chosen to give the desired value of the spontaneous polarization P_o. It can be easily shown that $\alpha_1 = 1/2\varepsilon_0\chi$, where ε_0 is the vacuum permittivity, χ is the susceptibility of the material. Negative α_1 values correspond to unstable parent paraelectric phases. Positive α_1 values correspond to stable or metastable parent phases, depending on the relative relation among α_1, α_{11}, and α_{111}. Namely, when $\alpha_{11}^2 > 3\alpha_1\alpha_{111}$, the parent phase is metastable, otherwise it is stable. In this paper, as in Ref. 6, negative α_{11} is employed to describe a first-order transition. Since the ferroelectric state is of tetragonal structure, the vector field takes one of the six states $\mathbf{P} = P_o(1, 0, 0)$, $P_o(-1, 0, 0)$, $P_o(0, 1, 0)$, $P_o(0, -1, 0)$, $P_o(0, 0, 1)$, $P_o(0, 0, -1)$.

At the ferroelectric domain boundaries, it is assumed that the polarization fields vary continuously across boundaries. In the Ginzburg–Landau free-energy model, the domain wall energy is introduced through gradients of the polarization field. For a cubic system[10]

$$\begin{aligned} f_G(P_{i,j}) = {} & \frac{1}{2}G_{11}(P_{x,x}^2 + P_{y,y}^2 + P_{z,z}^2) \\ & + G_{12}(P_{x,x}P_{y,y} + P_{y,y}P_{z,z} + P_{z,z}P_{x,x}) \\ & + \frac{1}{2}G_{44}[(P_{x,y} + P_{y,x})^2 + (P_{y,z} + P_{z,y})^2 + (P_{z,x} + P_{x,z})^2] \\ & + \frac{1}{2}G'_{44}[(P_{x,y} - P_{y,x})^2 + (P_{y,z} - P_{z,y})^2 + (P_{z,x} - P_{x,z})^2] \end{aligned} \tag{2}$$

where $P_{i,j} = \partial P_i/\partial x_j$. For a generic choice of G_{11}, G_{12}, G_{44}, and G'_{44}, the domain wall energy is not isotropic.

Cubic–tetragonal displacive phase transitions are structural transformations involving a change of crystal structures and lattice parameters. If we assume that the boundaries between the parent paraelectric phase and the product ferroelectric phase as well as the boundaries between the different orientation domains of the ferroelectric phase are coherent, elastic strain energy will be generated during the phase transition in order to accommodate the structural changes. We assume that the local elastic strain generated during the phase transition has a linear-quadratic coupling with the local polarization field. This coupling results in the so-called electrostrictive energy[9]

$$\begin{aligned} f_{es}(P_i,\eta_{ij}) = {} & -q_{11}(\eta_{xx}P_x^2 + \eta_{yy}P_y^2 + \eta_{zz}P_z^2) \\ & - q_{12}[\eta_{xx}(P_y^2 + P_z^2) + \eta_{yy}(P_x^2 + P_z^2) + \eta_{zz}(P_x^2 + P_y^2)] \\ & - 2q_{44}(\eta_{xy}P_xP_y + \eta_{xz}P_xP_z + \eta_{yz}P_yP_z) \end{aligned} \tag{3}$$

where q_{ij} are the electrostrictive constants and $\eta_{ij} = \frac{1}{2}(u_{i,j} + u_{j,i})$ is the linear elastic strain, u_i is elastic displacement. The corresponding elastic energy density reads

$$\begin{aligned} f_{\text{ela}}(\eta_{ij}) = {} & \frac{1}{2}C_{11}(\eta_{xx}^2 + \eta_{yy}^2 + \eta_{zz}^2) + C_{12}(\eta_{xx}\eta_{yy} + \eta_{yy}\eta_{zz} \\ & + \eta_{zz}\eta_{xx}) + 2C_{44}(\eta_{xy}^2 + \eta_{yz}^2 + \eta_{zx}^2) \end{aligned} \tag{4}$$

where C_{ij}'s are the second-order elastic constants.

And finally, for an inhomogeneous system, we have to consider the long-range electric dipole–dipole interactions. In SI units, it takes the familiar form

$$\begin{aligned} F_{\text{dip}}\{P_i\} = {} & \frac{1}{8\pi\varepsilon_0}\int\int d^3\mathbf{r}_i d^3\mathbf{r}_j \\ & \left\{\frac{\mathbf{P}(\mathbf{r}_i)\cdot\mathbf{P}(\mathbf{r}_j)}{|\mathbf{r}_i - \mathbf{r}_j|^3} - \frac{3[\mathbf{P}(\mathbf{r}_i)\cdot(\mathbf{r}_i - \mathbf{r}_j)][\mathbf{P}(\mathbf{r}_j)\cdot(\mathbf{r}_i - \mathbf{r}_j)]}{|\mathbf{r}_i - \mathbf{r}_j|^5}\right\} \end{aligned} \tag{5}$$

We will see that it is this interaction which is responsible to the head-to-tail arrangement of dipoles at the twin boundaries.

We can also write Eq. (5) as

$$F_{\text{dip}}\{P_i\} = \frac{1}{2}\int d^3\mathbf{r}_i\mathbf{E}_1(\mathbf{r}_i)\cdot\mathbf{P}(\mathbf{r}_i) \tag{6}$$

where

$$\mathbf{E}_1(\mathbf{r}_i) = \frac{1}{4\pi\varepsilon_0}\int d^3\mathbf{r}_j\left\{\frac{\mathbf{P}(\mathbf{r}_j)}{|\mathbf{r}_i - \mathbf{r}_j|^3} - \frac{3[(\mathbf{r}_i - \mathbf{r}_j)][\mathbf{P}(\mathbf{r}_j)\cdot(\mathbf{r}_i - \mathbf{r}_j)]}{|\mathbf{r}_i - \mathbf{r}_j|^5}\right\} \tag{7}$$

is the electric field caused by the dipole moments of all other dipoles in the specimen. Contributing to this field are the surface charges on the boundary. The electric field caused by surface charges is called the depolarization field.

Let's write

$$\mathbf{P}(\mathbf{r}) = \overline{\mathbf{P}} + \delta\mathbf{P}(\mathbf{r}) \tag{8}$$

where $\overline{\mathbf{P}}$ is the spatially independent average polarization and $\delta\mathbf{P}$ is the spatially dependent heterogeneous part of the polarization field. The average field $\overline{\mathbf{P}}$ is defined in such a way that $\int \delta\mathbf{P}(\mathbf{r})d^3\mathbf{r} = 0$. Substituting Eq. (11) into Eq. (5), we have

$$F_{\text{dip}}\{P_i\} = F_{\text{dip}}\{\overline{P}_i\} + F_{\text{dip}}^{\text{cr}}\{\overline{P}_i,\delta P_i\} + F_{\text{dip}}\{\delta P_i\} \tag{9}$$

where

$$\begin{aligned} F_{\text{dip}}\{\overline{P}_i\} = {} & \frac{1}{8\pi\varepsilon_0}\int\int d^3\mathbf{r}_i d^3\mathbf{r}_j \\ & \left\{\frac{\overline{\mathbf{P}}\cdot\overline{\mathbf{P}}}{|\mathbf{r}_i - \mathbf{r}_j|^3} - \frac{3[\overline{\mathbf{P}}\cdot(\mathbf{r}_i - \mathbf{r}_j)][\overline{\mathbf{P}}\cdot(\mathbf{r}_i - \mathbf{r}_j)]}{|\mathbf{r}_i - \mathbf{r}_j|^5}\right\} \end{aligned} \tag{10}$$

is the part of the contribution from the average polarization

$$\begin{aligned} F_{\text{dip}}^{\text{cr}}\{\overline{P}_i,\delta P_i\} = {} & \frac{1}{4\pi\varepsilon_0}\int\int d^3\mathbf{r}_i d^3\mathbf{r}_j \\ & \left\{\frac{\overline{\mathbf{P}}\cdot\delta\mathbf{P}(\mathbf{r}_j)}{|\mathbf{r}_i - \mathbf{r}_j|^3} - \frac{3[\overline{\mathbf{P}}\cdot(\mathbf{r}_i - \mathbf{r}_j)][\delta\mathbf{P}(\mathbf{r}_j)\cdot(\mathbf{r}_i - \mathbf{r}_j)]}{|\mathbf{r}_i - \mathbf{r}_j|^5}\right\} \end{aligned} \tag{11}$$

is the cross term, and

$$F_{\text{dip}}\{\delta P_i\} = \frac{1}{8\pi\varepsilon_0}\int\int d^3\mathbf{r}_i d^3\mathbf{r}_j \left\{\frac{\delta\mathbf{P}(\mathbf{r}_i)\cdot\delta\mathbf{P}(\mathbf{r}_j)}{|\mathbf{r}_i-\mathbf{r}_j|^3} - \frac{3[\delta\mathbf{P}(\mathbf{r}_i)\cdot(\mathbf{r}_i-\mathbf{r}_j)][\delta\mathbf{P}(\mathbf{r}_j)\cdot(\mathbf{r}_i-\mathbf{r}_j)]}{|\mathbf{r}_i-\mathbf{r}_j|^5}\right\} \tag{12}$$

is the contribution of the spatially dependent part of the polarization field.

We can rewrite Eqs. (10)–(12) in Fourier space. For $F_{\text{dip}}\{\delta P_i\}$:[5]

$$F_{\text{dip}}\{\delta P_i\} = \frac{1}{2\varepsilon_0}\int\frac{d^3\mathbf{k}}{(2\pi)^3}\frac{|\delta\mathbf{P}(\mathbf{k})\cdot\mathbf{k}|^2}{k^2} = \frac{1}{2\varepsilon_0\chi}\int\frac{d^3\mathbf{k}}{(2\pi)^3}|\delta\mathbf{P}(\mathbf{k})\cdot\mathbf{n}|^2 \tag{13}$$

where

$$\delta\mathbf{P}(\mathbf{k}) = \int d^3\mathbf{r}\delta\mathbf{P}(\mathbf{r})e^{-i\mathbf{k}\cdot\mathbf{r}} \tag{14}$$

is the Fourier transform of the spatially dependent part of the polarization field $\delta P(\mathbf{r})$, and $\mathbf{n} = (n_1, n_2, n_3)$, $n_i = k_i/|\mathbf{k}|(i = 1, 2, 3)$ is the unit vector in the reciprocal space. It should be noted that

$$\delta\mathbf{P}(\mathbf{k}) = \begin{cases} 0, & \mathbf{k} = 0 \\ \mathbf{P}(\mathbf{k}), & \mathbf{k} \neq 0 \end{cases} \tag{15}$$

In Fourier space, the contribution from the average polarization and the cross term can be written as follows:

$$F_{\text{dip}}\{\overline{P}\} = \frac{1}{2\varepsilon_0}\overline{P}_i\overline{P}_j\int d^3\mathbf{r}d^3\mathbf{k}\delta(\mathbf{k})e^{i\mathbf{k}\cdot\mathbf{r}}n_i n_j \tag{16}$$

$$F^{\text{cr}}_{\text{dip}}\{\overline{P}_i,\delta P_i\} = \frac{1}{\varepsilon_0}\overline{P}_i\int\frac{d^3\mathbf{k}}{(2\pi)^3}\delta(\mathbf{k})\delta P_j(\mathbf{k})n_i n_j \tag{17}$$

where

$$\delta(\mathbf{k}) = \begin{cases} 1, & \mathbf{k} = 0 \\ 0, & \mathbf{k} \neq 0 \end{cases} \tag{18}$$

It is easy to see that

$$F^{\text{cr}}_{\text{dip}}\{\overline{P}_i,\delta P_i\} = 0 \tag{19}$$

For the contribution from average polarization, $F_{\text{dip}}\{\overline{P}_i\}$, Eq. (16) is not well defined at $\mathbf{k} = 0$. However, according to Ref. 11, the depolarization field caused by a uniform polarization is given by

$$\mathbf{E}_{\text{dep}} = -\frac{1}{\varepsilon_0}\overline{\mathbf{P}} \tag{20}$$

the corresponding depolarization energy is

$$\begin{aligned} F_{\text{dep}}\{P_i\} &= -\frac{1}{2}\int d^3\mathbf{r}\mathbf{E}_{\text{dep}}\cdot\mathbf{P} \\ &= \frac{1}{2\varepsilon_0}\overline{P}_i\int d^3\mathbf{r}P_i \\ &= \frac{1}{2\varepsilon_0}\overline{P}_i\overline{P}_i\int d^3\mathbf{r} \end{aligned} \tag{21}$$

since $\int d^3\mathbf{r}P_i = V\overline{P}_i = \overline{P}_i\int d^3\mathbf{r}$, where V is the volume of the specimen.

Therefore, we have

$$F_{\text{dip}}\{P_i\} = F_{\text{dip}}\{\delta P_i\} + F_{\text{dep}}\{P_i\} \tag{22}$$

It will be shown that when $F_{\text{dep}}\{P_i\}$ is taken into account, 180° degree domains are favored. As a result, both 180° and 90° domains remain stable in a clamped system without free charge carriers.

In summary, the total free energy of a system with a domain structure is the sum of the Landau bulk free energy F_{L}, the gradient energy F_{G}, the electrostrictive energy F_{es}, the elastic energy F_{ela}, the energy due to the long-range electric dipole–dipole interaction $F_{\text{dip}}\{P_i\}$—which can be written as the spatially dependent part $F_{\text{dip}}\{P_i^{\text{s}}\}$ and the depolarization energy F_{dep}:

$$\begin{aligned} F(\{P_i\},\{P_{i,j}\},\{\eta_{ij}\}) &= F_{\text{L}}\{P_i\} + F_{\text{G}}\{P_{i,j}\} + F_{\text{es}}(\{P_i\},\{\eta_{ij}\}) \\ &\quad + F_{\text{ela}}\{\eta_{ij}\} + F_{\text{dip}}\{P_i\} \\ &= \int d^3\mathbf{r}[f_{\text{L}}(P_i) + f_{\text{G}}(P_{i,j}) + f_{\text{es}}(P_i,\eta_{ij}) \\ &\quad + f_{\text{ela}}(\eta_{ij})] + F_{\text{dip}}\{\delta P_i\} + F_{\text{dep}} \end{aligned} \tag{23}$$

It should be pointed out that although the elastic strain energy appears in the total free energy (Eq. (23)) as a volume integral of an elastic strain energy density function, minimization of the total free energy with respect to elastic strain immediately results in nonlocal elastic interactions between the volume elements of a domain structure described by a nonequilibrium polarization field.

III. Elastic Strain Energy of a Domain Structure

In the model given in the previous section, both the polarization field and the linear elastic strain field appear as order parameters. However, one may assume that the mechanical relaxation of an elastic field is much faster than the electric relaxation of a polarization field. Consequently, during the process of ferroelectric transition, the system in question reaches its mechanical equilibrium instantaneously at every stage. This assumption enables us to eliminate the elastic strain field using the static condition of mechanical equilibrium. Therefore, the elastic strain energy of a domain structure becomes a function of the polarization field.

For a stress-free homogeneous system, minimization of the total free energy with respect to the elastic strain results in a simple renormalization of the constants α_{11} and α_{12} of the fourth-order terms in the Landau free energy. This renormalization usually produces a stronger first-order phase transition.

For an inhomogeneous system, the elastic strain field can be written as a sum of a spatially independent homogeneous strain, $\overline{\eta}_{i,j}$, and a spatially dependent heterogeneous strain field $\delta\eta_{i,j}$. The homogeneous strain determines the macroscopic shape deformation of the crystal as a whole produced by internal stress due to the presence of domain structures. The heterogeneous strain is defined in such a way that

$$\int\delta\eta_{i,j}d^3\mathbf{r} = 0 \tag{24}$$

If there is no external stress applied and the crystal is unconstrained with respect to the macroscopic deformation, the equilibrium deformation due to the formation of a given domain structure is obtained by minimizing the total energy of the system with respect to the homogeneous strain.

$$\begin{aligned} \overline{\eta}_{xx} &= Q_{11}\overline{P_x^2} + Q_{12}(\overline{P_y^2} + \overline{P_z^2}) \\ \overline{\eta}_{yy} &= Q_{11}\overline{P_y^2} + Q_{12}(\overline{P_x^2} + \overline{P_z^2}) \\ \overline{\eta}_{zz} &= Q_{11}\overline{P_z^2} + Q_{12}(\overline{P_x^2} + \overline{P_y^2}) \\ \overline{\eta}_{yz} &= (q_{44}/(2C_{44}))\overline{P_yP_z} \\ \overline{\eta}_{xz} &= [q_{44}/(2C_{44})]\overline{P_xP_z} \\ \overline{\eta}_{xy} &= [q_{44}/(2C_{44})]\overline{P_xP_y} \end{aligned} \tag{25}$$

where $\overline{P_i^2}$ and $\overline{P_iP_j}$ represent the volume averages over a system containing domain structures, and

$$Q_{11} = \frac{1}{3}\left(\frac{q_{11}+2q_{12}}{C_{11}+2C_{12}} + 2\,\frac{q_{11}-q_{12}}{C_{11}-C_{12}}\right)$$

$$Q_{12} = \frac{1}{3}\left(\frac{q_{11}+2q_{12}}{C_{11}+2C_{12}} - \frac{q_{11}-q_{12}}{C_{11}-C_{12}}\right) \tag{26}$$

The elastic energy and electrostrictive energy due to the homogeneous deformation can be obtained by substituting the equilibrium homogeneous strain (Eq. (25)) back to the elastic strain energy expression f_{ela} and the electrostrictive energy expression f_{es}. They depend on the volume fractions of each orientation domain. On the other hand, if the boundary is clamped instead of stress-free, the homogeneous deformation is prohibited and the corresponding homogeneous strain is zero.

The equilibrium heterogeneous strain field $\delta\eta_{i,j}$ satisfies the mechanical equilibrium condition given by the Euler equation with respect to the elastic displacement

$$\sigma_{ij,j} = 0,\ (i, j = 1, 2, 3) \tag{27}$$

where

$$\sigma_{ij} = \frac{\delta F}{\delta \eta_{ij}} \tag{28}$$

is the Cauchy stress tensor, F is the total free-energy functional.

For the case of homogeneous modulus approximation, the equilibrium Eq. (27) can be readily solved in Fourier space. Details of the derivation can be found in Ref. 5. The sum of elastic strain energy and the electrostrictive energy due to the heterogeneous strain relaxation is given by

$$F_{\text{het}} = -\frac{1}{2}\int \frac{d^3\mathbf{k}}{(2\pi)^3}\left[n_i \Gamma_{ij}(\mathbf{k})\Omega_{jl}(\mathbf{n})\Gamma^*_{lm}(\mathbf{k})n_m\right] \tag{29}$$

where $\Gamma_{ij}(\mathbf{k})$ are Fourier transforms of $\Gamma_{ij}(\mathbf{r})$, which in turn are given by

$$\begin{aligned}
\Gamma_{11} &= q_{11}P_x^2 + q_{12}(P_y^2 + P_z^2)\\
\Gamma_{22} &= q_{11}P_y^2 + q_{12}(P_x^2 + P_z^2)\\
\Gamma_{33} &= q_{11}P_z^2 + q_{12}(P_x^2 + P_y^2)\\
\Gamma_{12} &= \Gamma_{21} = 2q_{44}P_xP_y\\
\Gamma_{23} &= \Gamma_{32} = 2q_{44}P_yP_z\\
\Gamma_{31} &= \Gamma_{13} = 2q_{44}P_xP_z
\end{aligned} \tag{30}$$

Ω_{jm} is given by

$$\Omega_{ii}(n) = \frac{C_{44} + (C_{11}-C_{44})(n_j^2+n_k^2) + \zeta(C_{11}+C_{12})n_j^2n_k^2}{C_{44}D(n)}$$

$$\Omega_{ij}(n) = -\frac{(C_{12}+C_{44})(1+\zeta n_k^2)}{C_{44}D(n)}\,n_in_j \tag{31}$$

where indexes i, j, k form a cyclic sequence

$$\zeta = (C_{11} - C_{12} - 2C_{44})/C_{44} \tag{32}$$

is the elastic anisotropy and

$$\begin{aligned}
D(\mathbf{n}) = {} & C_{11} + \zeta(C_{11}+C_{12})(n_2^1n_2^2 + n_1^2n_3^2 + n_2^2n_3^2)\\
& + \zeta^2(C_{11}+2C_{12}+C_{44})n_1^2n_2^2n_3^2
\end{aligned} \tag{33}$$

It can be easily shown that by converting the expression for the elastic strain energy and the electrostrictive energy (Eq. (29)) from Fourier space to the real space, the elastic interactions are nonlocal and highly anisotropic.

IV. Domain Evolution Equation

The three components of the polarization vector represent three nonconserved order parameter fields since the volume fraction of each orientation domain is not constant during the evolution of a domain structure. The temporal relaxation of nonconserved fields is described by the TDGL equations,[12] i.e.

$$\frac{\partial}{\partial t}P_i(\mathbf{r},t) = -L\frac{\delta F'}{\delta P_i(\mathbf{r},t)} + \xi_i(\mathbf{r},t) \tag{34}$$

where F' is the total free-energy functional after eliminating the elastic field, and $\xi_i(\mathbf{r},t)$ is the Gaussian random fluctuation satisfying

$$\begin{aligned}
&\langle \xi_i(\mathbf{r},t)\rangle = 0\\
&\langle \xi_i(\mathbf{r},t)\xi_j(\mathbf{r}',t')\rangle = 2k_BTL\delta_{ij}\delta(\mathrm{r}=\mathbf{r}')\delta(t-t')
\end{aligned} \tag{35}$$

where k_B is the Boltzman constant, T is temperature, δ_{ij} is the Kronecker symbol, and $\delta(\mathbf{r}-\mathbf{r}')$ is the delta function. The bracket $\langle . . \rangle$ denotes an average over fluctuations of all the $\xi_i(\mathbf{r},t)$.

The temporal evolution of the polarization vector fields, and thus the domain structures, is obtained by numerically solving the TDGL equations. Since the elastic strain energy and the electrostrictive energy due to the heterogeneous strain field have a single analytical expression as a function of the polarization field in Fourier space, the computer simulation is most conveniently performed directly in the reciprocal space. Furthermore, in Fourier-transforming the TDGL equation, one must transform $\delta F/\delta P_i$ instead of F to reciprocal space.

V. Semi-Implicit Fourier-Spectral Method

In the present work, the TDGL equations are numerically solved in the Fourier space, in which both the elastic and electric dipole–dipole interactions have analytical forms. We use the semi-implicit Fourier-spectral method,[13] which enables us to increase the time step considerably.

We can rewrite Eq. (34) as

$$\frac{\partial}{\partial t}P_i(\mathbf{r},t) = -L\frac{\delta F''}{\delta P_i(\mathbf{r},t)} - L\frac{\delta F_G}{\delta P_i(\mathbf{r},t)} + \xi_i(\mathbf{r},t) \tag{36}$$

where $F_G = \int d^3\mathbf{r} f_G(P_{i,j})$ is the gradient energy term, and $F'' = F' - F_G$ is the free energy including elastic energy and excluding the gradient energy part.

In Fourier space, the TDGL equations read

$$\frac{\partial}{\partial t}\tilde{P}_i(\mathbf{k},t) = -L\{f(P_j)\}_{\mathbf{k}} - G_i\tilde{P}_i(\mathbf{k},t) + \xi_i(\mathbf{r},t) \tag{37}$$

where $\tilde{P}_i(\mathbf{k},t)$ and $\{\tilde{f}(P_i)\}_{\mathbf{k}}$ are the Fourier transforms of $P_i(\mathbf{r},t)$ and $\delta F''/\delta P_i(\mathbf{r},t)$, respectively. G_i's are the gradient operators corresponding to the ith-component of the polarization field, as defined as follows:

$$\begin{aligned}
G_1 &= G_{11}k_1^2 + (G_{44}+G'_{44})(k_2^2+k_3^2)\\
G_2 &= G_{11}k_2^2 + (G_{44}+G'_{44})(k_1^2+k_3^2)\\
G_3 &= G_{11}k_3^2 + (G_{44}+G'_{44})(k_1^2+k_2^2)
\end{aligned} \tag{38}$$

The explicit Euler Fourier-spectral method is to approximate the above equations by the explicit Euler scheme

$$\tilde{P}_i^{n+1}(\mathbf{k},t) = \tilde{P}_i^n(\mathbf{k},t) + \Delta t[\{\tilde{f}(P_j^n)\}_{\mathbf{k}} - G_i\tilde{P}_i^n(\mathbf{k},t)] \tag{39}$$

In this work, we employ the semi-implicit scheme proposed in Ref. 13.

$$(1+\Delta tG_i)\tilde{P}_i^{n+1}(\mathbf{k},t) = \tilde{P}_i^n(\mathbf{k},t) + \Delta t\{\tilde{f}(P_k^n)\}_{\mathbf{k}} \tag{40}$$

Since Eq. (40) is only first-order accurate in time, it is not sufficient for time-dependent solutions. In this case, higher-

order semi-implicit schemes are needed. The second-order scheme is given by

$$(3 + 2\Delta t G_i)\tilde{P}_i^{n+1}(\mathbf{k},t) = 4\tilde{P}_i^{n}(\mathbf{k},t) - \tilde{P}_i^{n-1}(\mathbf{k},t) + 2\Delta t[2\{\tilde{f}(P_j^n)\}_{\mathbf{k}} - \{\tilde{f}(P_j^{n-1})\}_{\mathbf{k}}] \quad (41)$$

The third-order scheme is

$$(11 + 6\Delta t G_i)\tilde{P}_i^{n+1}(\mathbf{k},t) = 18\tilde{P}_i^{n}(\mathbf{k},t) - 9\tilde{P}_i^{n-1}(\mathbf{k},t) + 2\tilde{P}_i^{n-2}(\mathbf{k},t) + 6\Delta t[3\{\tilde{f}(P_j^n)\}_{\mathbf{k}} - 3\{\tilde{f}(P_j^{n-1})\}_{\mathbf{k}} + \{\tilde{f}(P_j^{n-1})\}_{\mathbf{k}}] \quad (42)$$

First, we use Eq. (40) to advance the first step, computing $\tilde{P}_i^1(\mathbf{k},t)$ and $\{\tilde{f}(P_j^1)\}_{\mathbf{k}}$. Then we use Eq. (41) to compute $\tilde{P}_i^2(\mathbf{k},t)$ and $\{\tilde{f}(P_j^2)\}_{\mathbf{k}}$. With these quantities, we start the iteration using Eq. (42).

This semi-implicit scheme enables us to increase the time step considerably without losing stability and accuracy. In the particular case at hand, we were able to increase the time step by five times compared to the explicit Euler method.

VI. Computer Simulation Results and Discussion

In the present work, we employ a $64 \times 64 \times 64$ lattice with periodic boundary conditions along the three Cartesian axes. The use of periodic boundary conditions imposes artificial periodicity of ferroelectric domains. This is particularly true when the domain size is comparable to the computational cell size. However, this artifact does not change the main conclusions of the paper. We consider only the clamped boundary condition in which the homogeneous strain is zero. The back-Fourier transform at a given step produces the real-space domain structures represented by the polarization fields.

Since, experimentally, barium titanate ($BaTiO_3$) is the most intensively studied ferroelectric material, the parameters of our model are chosen to correspond to those of $BaTiO_3$ (see, for example, Ref. 14). In particular, we choose $q_{11} = 14.2 \times 10^9$ $N{\cdot}m^2{\cdot}C^{-2}$, $q_{12} = -0.74 \times 10^9$ $N{\cdot}m^2{\cdot}C^{-2}$, $q_{44} = 1.57 \times 10^9$ $N{\cdot}m^2{\cdot}C^{-2}$, $C_{11} = 275 \times 10^9$ $N{\cdot}m^{-2}$, $C_{12} = 179 \times 10^9$ $N{\cdot}m^{-2}$, and $C_{44} = 54.3 \times 10^9$ $N{\cdot}m^{-2}$.

We employ the same set of the dimensionless variables as used in the 2-D case.[6] Since α_1, L, and G_{11} have units of $C^{-2}{\cdot}m^2{\cdot}N$, $s^{-1}{\cdot}m^{-2}{\cdot}C^2{\cdot}N^{-1}$, and $C^{-2}{\cdot}m^4{\cdot}N$, respectively, it is clear that $\sqrt{G_{11}/|\alpha_1|}$ and $1/(|\alpha_1|L)$ have the dimensions of distance and time, respectively. So a natural choice of the dimensionless reduced variables is

$$\hat{\mathbf{r}} = \sqrt{|\alpha_1|/G_{11}}\mathbf{r}$$
$$\tau = |\alpha_1|Lt$$
$$\hat{\mathbf{P}} = \mathbf{P}/|\mathbf{P}_0| \quad (43)$$

Where $\mathbf{P}_0$ is the spontaneous polarization at a given temperature. In the reduced variables, the effective coefficients are related to the original ones as follows:

$$\alpha_1' = \alpha_1/|\alpha_1|$$
$$\alpha_{11}' = \alpha_{11}P_0^2/|\alpha_1|$$
$$\alpha_{12}' = \alpha_{12}P_0^2/|\alpha_1|$$
$$\alpha_{111}' = \alpha_{111}P_0^4/|\alpha_1|$$
$$\alpha_{112}' = \alpha_{112}P_0^4/|\alpha_1|$$
$$\alpha_{123}' = \alpha_{123}P_0^4/|\alpha_1|$$
$$g_{14} = (G_{11} + G_{44} - G_{44}')/G_{11}$$
$$g_{44} = (G_{44} + G_{44}')/G_{11}$$
$$q_{11}' = q_{11}/|\alpha_1|$$
$$q_{12}' = q_{12}/|\alpha_1|$$
$$q_{44}' = q_{44}/|\alpha_1|$$
$$C_{11}' = C_{11}/(|\alpha_1|P_0^2)$$
$$C_{12}' = C_{12}/(|\alpha_1|P_0^2)$$
$$C_{44}' = C_{44}/(|\alpha_1|P_0^2) \quad (44)$$

where $P_0 = |\mathbf{P}_0|$. It is clear that $\alpha_1' = -1.0$, since α_1 is negative in order to make the initial paraelectric phase unstable. In reduced variables, the lattice spacing in real space is chosen to be $\Delta x = 1.0$, the time step is $\Delta\tau = 0.05$. The values of other coefficients used in our simulation are given in Table I.

As mentioned before, the domain structure is represented by the polarization field, which at each lattice site is a three-component vector, whose magnitude and direction is represented by the length and the arrow direction of short lines. Since a 3-D picture of a $64 \times 64 \times 64$ grid involving vectors is difficult to visualize, in this paper we will use 2-D sections of the 3-D grid instead. Three sectional planes, namely, *xy*, *xz*, and *yz* planes are necessary to represent a 3-D grid. In this paper, the sections are chosen to be at the middle of the axis perpendicular to the plane. As a result, they share the same center point. The relative locations of these sectional planes are shown in Fig. 1(a).

To investigate the effect of the spatially dependent part of the dipole–dipole interaction energy and the depolarization energy on domain formation, we performed simulations with different energy terms taken into account. The evolution of morphologies are shown in Figs. 1–3. In each case, the initial condition is a high-temperature homogeneous paraelectric phase, created by assigning a zero value at each lattice site for each component of the polarization field. Since the coefficient α_1 in the Landau free-energy expression is chosen to be negative, the initial paraelectric phase is unstable with respect to the transition to the ferroelectric phase, and hence small random perturbations introduced to the initial uniform paraelectric state are sufficient to trigger the transition.

Figure 1 shows the temporal evolution of morphologies on the *xy*-, *xz*-, and *yz*-planar sections. Together they give a picture of the formation of a 3-D domain structure and its subsequent temporal evolution. Here both spartially dependent dipole–dipole interaction and the depolarization energy are absent. As a result, in this case, the interaction that governs the domain formation and evolution is just the elastic interaction. It takes about 10,000 time steps for stable morphologies to develop. Due to the absence of the dipole–dipole interaction, the fraction of head-to-head and tail-to-tail domain walls does not decrease with time. In fact, head-to-head and tail-to-tail domain walls persist even in the final morphologies.

Figure 2 shows the evolution of the sectional morphologies when the spatially dependent dipole–dipole interactions and elastic interactions are both taken into account. However, the depolarization energy due to the uniform average polarization, $F_{dep}\{P_i\}$ is not included in this simulation. This corresponds to

Table I. Values of Effective Coefficients Used in the Simulation

α_{11}'	α_{12}'	α_{111}'	α_{112}'	α_{123}'	g_{14}	g_{44}	q_{11}'	q_{12}'	q_{44}'	C_{11}'	C_{12}'	C_{44}'
–0.5	9.0	0.8	4.0	1.0	0.0	1.0	0.142	–0.0074	0.0157	2.75	1.79	0.543

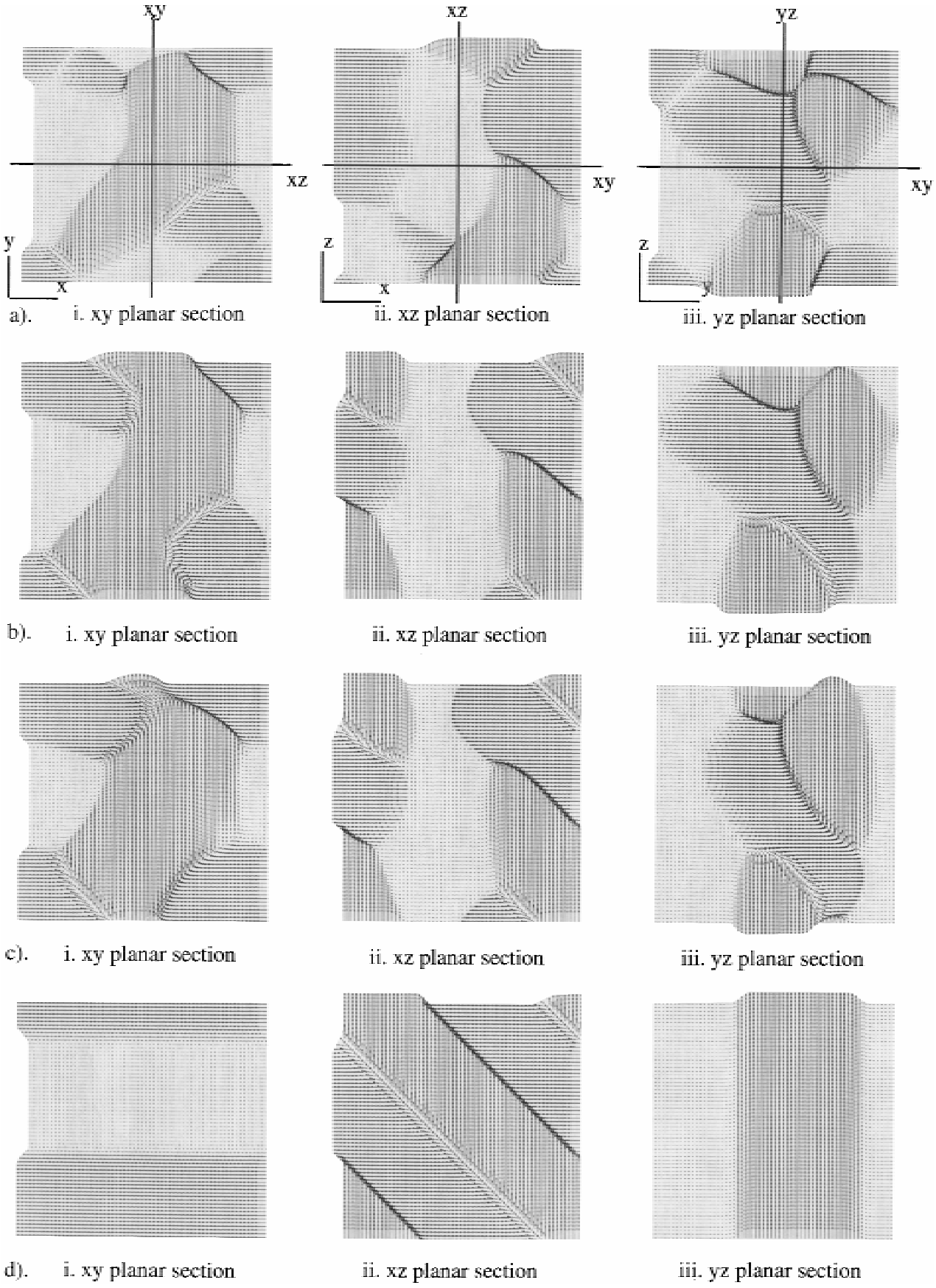

Fig. 1. Temporal evolution of sectional morphologies with elastic interaction, but without dipole–dipole interaction and depolarization energy. Head-to-head and tail-to-tail domains walls persist even at the final stages. (a) 1000 time steps; (b) 3000 time steps (c) 6000 time steps; (d) 10,000 time steps.

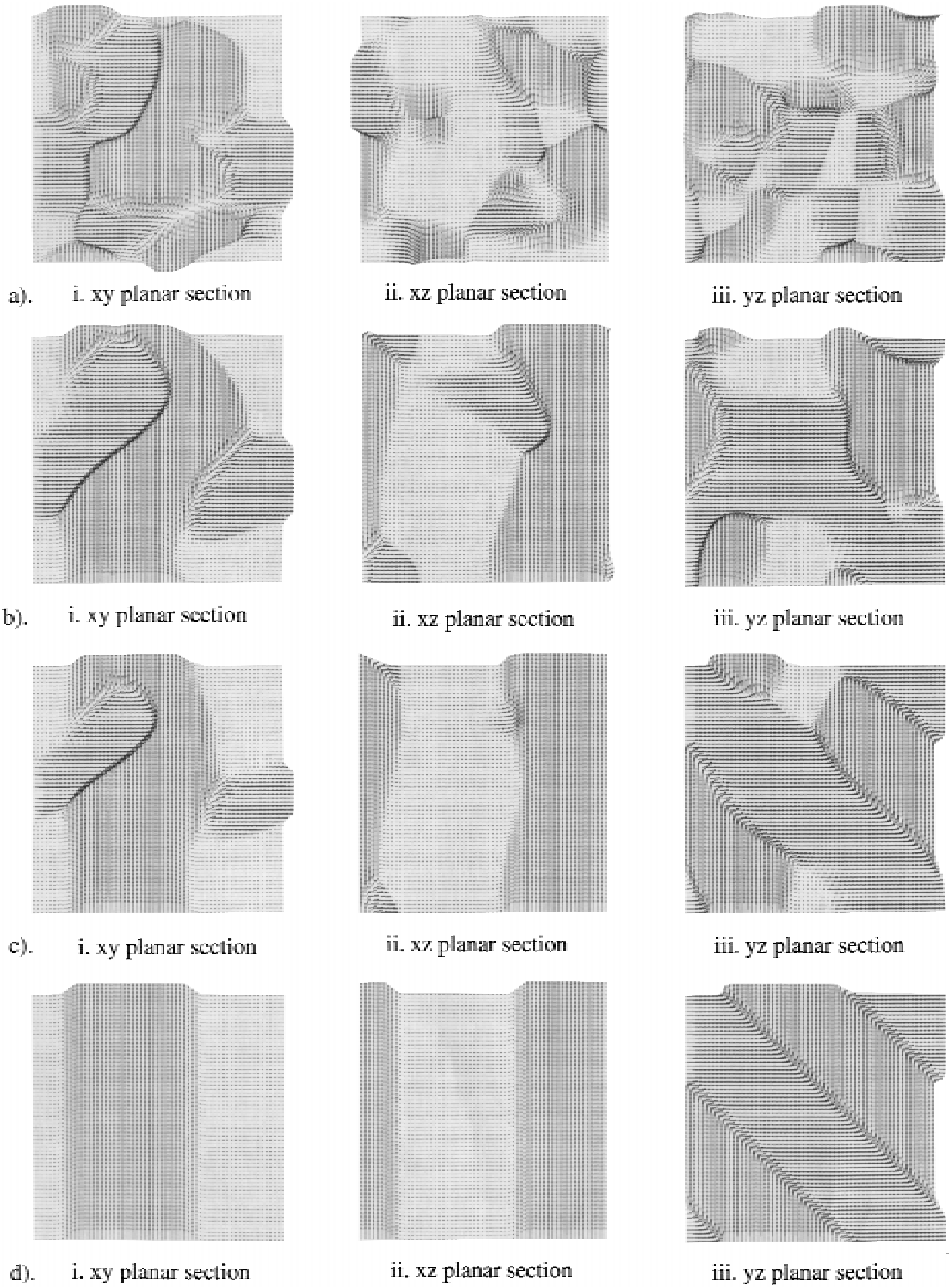

Fig. 2. Temporal evolution of sectional morphologies with both elastic interaction and dipole–dipole interaction, but without depolarization energy. The magnitude and the direction of polarization field are represented by the length and the arrow direction of a short line at each site. A dot at a site means the polarization is perpendicular to the plane at that site. (a) 500 time steps; (b) 1500 time steps; (c) 3000 time steps; (d) 5000 time steps.

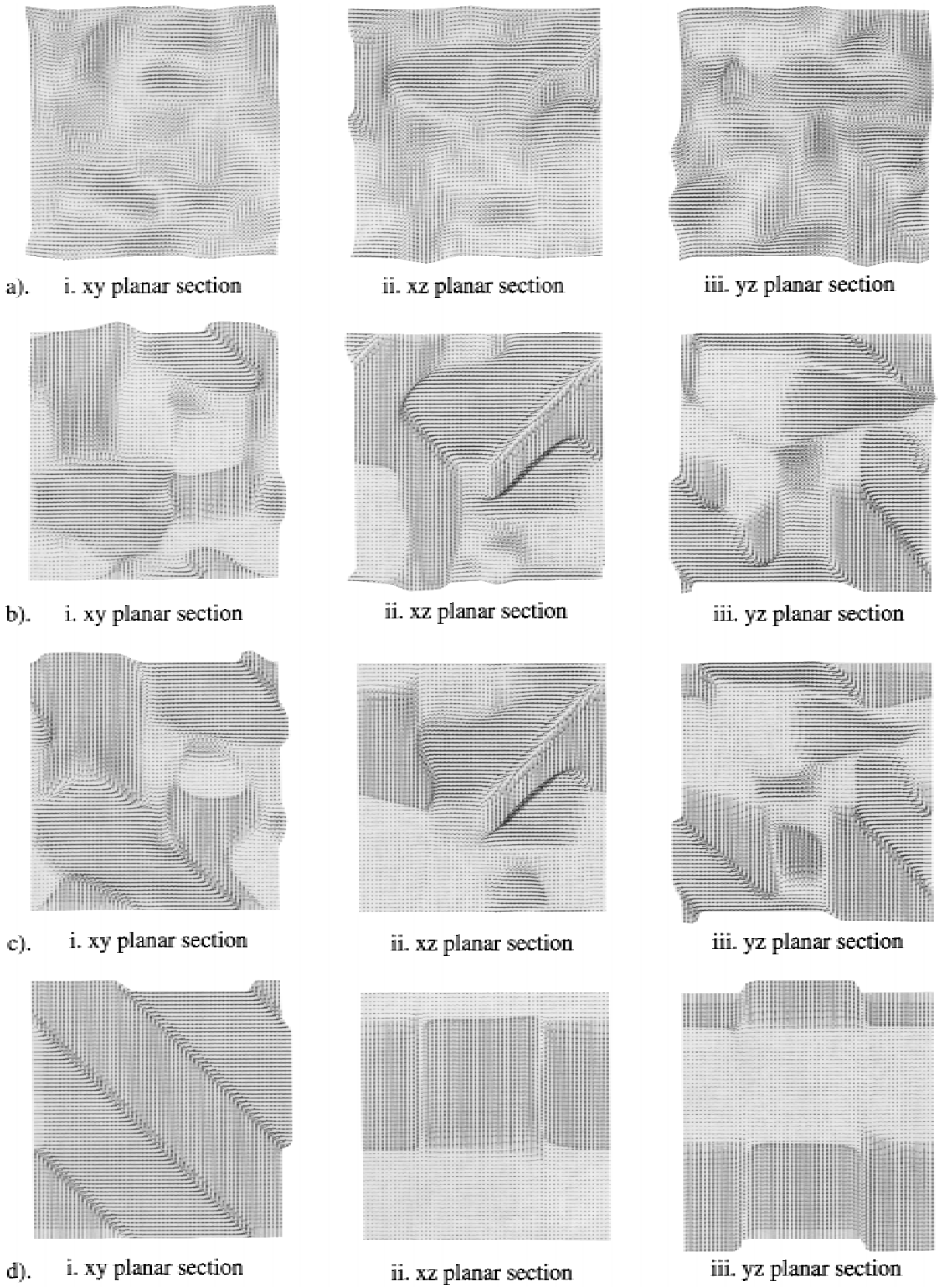

Fig. 3. Temporal evolution of sectional morphologies with elastic interactions, dipole–dipole interactions, and the depolarization energy term. When there is no homogeneous strain, which corresponds to a clamped system, both 180° and 90° domain are stable. (a) 1000 time steps; (b) 3000 time steps; (c) 6000 time steps; (d) 10,000 time steps.

the case when the polarization charges at the surface are totally compensated by free surface charges.

During the initial stages of domain coarsening after the system is transformed to the ferroelectric state, as can be seen in Fig. 2(a), all six different kinds of orientation domains allowed by symmetry are present. Furthermore, at the initial stage, both head-to-head and tail-to-tail arrangements of polarization fields across the domains walls are present. As time increases, the fraction of head-to-head and tail-to-tail domain walls decreases. Eventually, as shown in Fig. 2(d), only those domain walls with the head-to-tail arrangement survive. This result is consistent with the experimental observations.[1–3]

After about 3000 time steps (Fig. 2(c)), a strong alignment of domain walls along the [011] direction is developed. It should be noted that, in our simulation the gradient energy coefficients are chosen in such a way to provide the isotropic domain wall energy. As a result, the domain wall alignment is entirely due to the anisotropic and nonlocal elastic and electric dipole–dipole interactions. The three planar sections at 5000 steps are given in Fig. 2(d). The head-to-tail 90° domain structure is clearly shown in these figures.

This pattern of domain wall evolution, both in the presence of dipole–dipole interaction and in its absence, once again confirms our conclusion[6] that dipole–dipole interaction is responsible for the head-to-tail arrangement of dipoles across domain walls.

In Fig. 3, the domain evolution in the presence of both spatially dependent dipole–dipole energy and depolarization energy due to the uniform average polarization field is shown. In this case, both 90° and 180° domains develop as a result of the joint effect of the different interactions. Due to the presence of dipole–dipole interaction, at later stages, the head-to-tail arrangement of dipoles across domain walls is favored. Since the depolarization energy favors a configuration with vanished average polarization field, 180° domains develop in order to minimize the total free energy. However, because of geometric constraints, the 90° head-to-tail walls can be seen only in one of the three slice planes. Domain walls seen in the other slice planes are 180° walls. It seems also to be the case that the evolution of the domain structure to equilibrium is considerably slowed down due to the presence of the depolarization energy term.

In this case, it should be noted that, at the very last stage, the volume of the system where the polarization is along, say the $+z$ direction, is almost the same as that where the polarization is along the $-z$ direction, as can be clearly seen in Fig. 3(d). This configuration results in a vanishing average polarization field. This is indeed favored by the depolarization energy term (Eq. (10)), as the minimization of this term requires the average polarization field to have vanished.

From these simulations with different energy terms, it is clear that elastic interactions are critical to the formation of twin structure with domain walls along the [110] direction, dipole–dipole interactions are responsible for the head-to-tail arrangements of dipoles across the 90° walls along the [011] direction, and depolarization energy from the uniform average polarization field is the cause of the formation of stable 180° walls along the [100] direction.

VII. Summary

In conclusion, a comprehensive 3-D model of ferroelectric domain formation and evolution is formulated, based on the TDGL equations, which takes into account long-range electric dipole–dipole interaction energy, long-range elastic interaction energy, domain wall energy, depolarization energy, and short-range chemical interaction energy simultaneously. The 3-D simulation results using this model confirm our conclusions made in the 2-D case; namely, the nonlocal elastic interactions are critical to the formation of twin structure, and the dipole–dipole interactions arising from the heterogeneous polarization field are responsible for the head-to-tail arrangements of dipoles at twin boundaries.

It is also found that when there are no surface charges to compensate the Lorentz field due to the polarization charges, in addition to 90° domains, 180° domains are also stable features of a domain structure. This confirms that the depolarization energy is responsible for the appearance of stable 180° domains, since it is in favor of a vanishing average polarization field.

Acknowledgment: The authors are grateful for fruitful discussions with A. G. Khachaturyan and his suggestion for the depolarization energy.

References

[1]M. E. Lines and A. M. Glass, *Principles and Applications of Ferroelectrics and Related Materials.* Clarendon Press, Oxford, U.K., 1977.

[2]Y. Ishibashi, V. Janovec, R. Newnham, and V. Lemanov (Eds.), Special Issue on Domain Structures in Ferroelectrics, Ferroelastics, and Other Ferroic Materials, Parts I and II. *Ferroelectrics*, 97–98 (1989).

[3]J. C. Burfoot and G. W. Taylor, *Polar Dielectrics and Their Applications.* Macmillan, London, U.K., 1979.

[4]L. E. Cross, ''Ferroelectric Ceramics: Tailoring Properties for Specific Applications''; pp. 1–85 in *Ferroelectric Ceramics.* Birkhauser Verlag, Basel, Switzerland, 1993.

[5]A. G. Khachaturyan, *Theory of Structural Transformations in Solids*, Wiley, New York, 1983.

[6]H.-L. Hu and L. Q. Chen, ''Computer Simulation of 90° Ferroelectric Domain Formation and Evolution,'' *Mater. Sci. Eng. A.*, **238** [1] 182–89 (1997).

[7]W. Yang and L. Q. Chen, ''Computer Simulation of the Dynamics of 180° Ferroelectric Domains,'' *J. Am. Ceram. Soc.*, **78** [9] 2554–56 (1995).

[8]S. Nambu and D. A. Sagala, ''Domain Formation and Elastic Long-Range Interaction in Ferroelectric Perovskites,'' *Phys. Rev. B*, **50** [9] 5838–47 (1994).

[9](a) A. F. Devonshire, ''Theory of Ferroelectrics,'' *Adv. Phys.*, **3** [10] 85–130 (1954); (b) A. F. Devonshire, ''Theory of Titanate Part I,'' *Philos. Mag.*, **40** [7] 1040–63 (1949); (c) A. F. Devonshire, ''Theory of Titanate Part II,'' *Philos. Mag.*, **42** [7] 1065–79 (1951); (d) see also E. Fatuzzo and W. J. Merz, *Ferroelectricity*, North-Holland, Amsterdam, Wiley, New York, 1967.

[10]W. Cao and L. E. Cross, ''Theory of Tetragonal Twin Structures in Ferroelectric Perovskites with a First-order Phase Transition,'' *Phys. Rev. B*, **44** [1] 5–12 (1991).

[11]C. Kittel, *Introduction to Solid State Physics*, 6th ed. Wiley, New York, 1986.

[12]J. D. Gunton, M. San Miguel, and P. S. Sahni, in *Phase Transitions and Critical Phenomena*, Vol. 8. Edited by C. Domb and J. L. Lebowitz. Academic, New York, 1983.

[13]L. Q. Chen and J. Shen, ''Applications of Semi-Implicit Fourier-Spectral Method to Phase Field Equations,'' *Comput. Phys. Commun.*, 1997, in press.

[14](a) K. H. Hellwege and A. M. Hellwege (Eds.), *Elastic, Piezoelectric, Pyroelectric, Electrooptic Constants, and Nonlinear Dielectric Susceptibilities of Crystals*, Landolt-Börstein, New Series, Group 3, Vol. 11. Springer-Verlag, Berlin, Germany, 1979; (b) K. H. Hellwege and A. M. Hellwege (Eds.), *Ferroelectrics and Related Substances*, Landolt–Börstein, New Series, Group 3, Vol. 16, Pt. A. Springer-Verlag, Berlin, Germany, 1982. □